

ORIGINAL ARTICLE



Numerical assessment of stainless steel tubular T-joints subjected to brace and chord axial forces

Mateus M. Nogueira¹, Luciano R. O. de Lima², Pedro C. G. da S. Vellasco² and Ben Young³

Correspondence

Luciano R. O. de Lima
Structural Engineering Department,
UERJ – State University of Rio de Janeiro,
Brazil,
Email: luciano@eng.uerj.br

Affiliations

¹PGECIV - Civil Engineering Post-Graduate Program, UERJ – State University of Rio de Janeiro, Brazil

²Structural Engineering Department, UERJ – State University of Rio de Janeiro, Brazil

³Department of Civil and Environmental Engineering, The Hong Kong Polytechnic University, Hong Kong, China

Abstract

The utilisation of tubular sections in steel structures has increased significantly worldwide. The use of stainless steel provides several benefits for structures, including high corrosion resistance, durability, fire resistance and ease of maintenance. A significant issue in the design of tubular structures is the joints failure since they are highly susceptible to local failures that influence their actual overall behavior. The design rules of welded carbon steel tubular joints are available, such as Eurocode 3, part 1-8, NBR 16239, ISO 14346 and CIDECT guides. When stainless steel tubular joints are considered, the AS/NZS 4673 Australian/New Zealand Standard is the only available specification that can be used. An experimental and numerical analysis of these tubular joints are recommended since they enable a more accurate evaluation of their structural performance. Concerning these aspects, this work aims to investigate stainless steel tubular T-joints fabricated by SHS and RHS cold-formed profiles that focused on the effect of chord pre-loading. For this purpose, a numerical study based on finite element analysis was performed. The finite element model was developed and calibrated against experiments. The results were subsequently compared with the aforementioned design predictions.

Keywords

Stainless steel, tubular joints, numerical models, finite element analysis

1 Introduction

Tubular profiles have been increasingly used in steel structures due to its several structural benefits and aesthetic features. Nature confirms the excellent properties of tubular shapes when loaded in tension, compression, torsion or bending in any direction. Besides that, the profile closed geometry is associated with a smaller unprotected surface area, which increases the corrosion protection life of structures [1]. Despite the advantages of tubular sections, the joints in tubular structures may still represent a critical issue with numerous studies indicating that further research is needed, particularly for some geometries [2]. Stainless steel is used as a general expression to describe corrosion-resistant iron alloys that contain a minimum of 10.5% chromium. It has been traditionally regarded as an extravagant solution to structural engineering problems. Consequently, the use of stainless steel as a primary structural material for conventional construction remains somewhat limited [3]. Following Gardner [3], for the last 80 years, the longevity and aesthetic appeal of stainless steel have inspired architects and designers alike to use the material in both practical and imaginative ways. In the past, some experimental results on the effect of the chord stresses over the brace load capacity were published. These results showed that compressive chord stresses considerably decrease the joint resistance. However, very few studies indicated the same reduction in load-carrying capacity for joints under the action of chord tension forces. This trend is

reflected in EN 1993-1-8 [4] and ABNT NBR 16239 [5] design codes. At this point, it is necessary to observe that the second edition of the CIDECT design guide for RHS joints [6] and ISO 14346 [7] preconise some joint resistance reduction for both cases, i.e., tensile and compressive chord stresses. Experimental investigation of stainless steel cold-formed tubular T joints fabricated from the square and rectangular hollow section brace and chord members were conducted by Feng and Young [8]. A total of 22 tests were performed considering high strength stainless steel and normal strength stainless steel specimens, with the ratio of the brace width to chord width (β) varying from 0.5 to 1.0. In addition, Feng and Young [9] also proposed design rules for the different failure modes that can occur based on a numerical study of cold-formed stainless steel tubular T-joints and X-joints.

The finite element method is commonly used to reproduce the experiments performed in civil engineering laboratories and can well describe the nonlinear behaviour associated with stainless steel structures. Therefore, this paper is mainly focused on the numerical analysis of cold-formed stainless steel tubular T-joints with chord preload using the finite element method. This is followed by a comparison between strengths obtained from the parametric study and the current design rules in the Eurocode 3 part 1.8 [4] and the design rules proposed by Feng and Young [9].

2 Tubular joints design equations for sidewall failure mode

This study presents tubular square hollow sections (SHS) stainless steel T-joints with the ratio (β) of the brace width (b_1) to chord width (b_0) equal to 1.0, whose design is controlled by a sidewall failure. The actual design codes present equations for the resistance of carbon steel joints. Feng and Young [9] proposed design rules for stainless steel joints with no chord preload, altering the resistance of stainless-steel tubular T-joints present in Eurocode 3 part 1.8 (2010) [4] and CIDECT [10] with a α_B factor. Figure 1 shows the geometrical parameters for welded tubular T-joints, while the validity range of these geometric parameters is shown in Table 1.

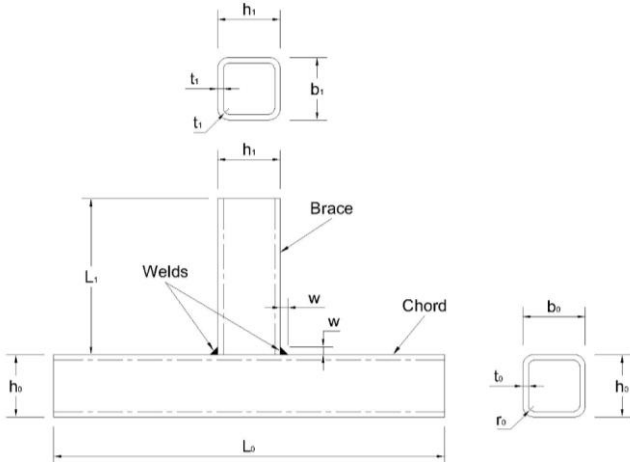


Figure 1 Definitions of the symbols for welded tubular T-joints

Table 1 Validity range of the geometric parameters

Geometric parameter	Eurocode 3	Parametric study and tests
$\beta = \frac{b_1}{b_0}$	[0.25-1.0]	1
$2\gamma = \frac{b_0}{t_0}$	≤ 35	[13.3-40.0]
$\frac{b_1}{t_1}$	≤ 35	[13.3-40.0]
$\frac{h_0}{t_0}$	≤ 35	[13.3-40.0]
$\frac{h_1}{t_1}$	≤ 35	[13.3-40.0]
$\frac{h_0}{b_0}$	[0.5-2.0]	1
$\frac{h_1}{b_1}$	[0.5-2.0]	1

If the parameters are following the design codes requirements, then the actual design Equations (1) to (8), presented below, for tubular T-joints can be used. The equations from Eurocode 3 part 1.8 [4] and CIDECT [10] predict the resistance related to the chord side wall failure mode:

$$N_{1,Rd} \geq N_{1,Ed} \quad (1)$$

$$N_{1,Rd} = \frac{k_n \cdot f_b \cdot t_0}{\sin \theta_1} \cdot \left(\frac{2 \cdot h_1}{\sin \theta_1} + 10 \cdot t_0 \right) \quad (2)$$

For tension:

$$f_b = f_{y0} \quad (3)$$

For compression:

$$f_b = \chi \cdot f_{y0} \quad (4)$$

where $N_{1,Ed}$ is the design value of the internal axial force at the brace, $N_{1,Rd}$ is the joint design resistance, θ_1 is the angle between the brace and the chord, f_{y0} is the chord yield stress and χ is the reduction factor for flexural buckling obtained from the buckling curve present in Eurocode 3 part 1.1 [11]. In that case, the buckling curve "c" must be used to calculate the reduction factor, because the concerned tubular joints are cold-formed. The normalised slenderness is determined from:

$$\bar{\lambda} = 3.46 \times \frac{\left(\frac{h_0}{t_0} - 2 \right) \cdot \sqrt{\frac{1}{\sin \theta_1}}}{\pi \cdot \sqrt{\frac{E}{f_{y0}}}} \quad (5)$$

where E is the elastic modulus, k_n is a factor that depends on n , that can be determined as a function of the chord maximum compressive stress ($\sigma_{0,Ed}$), as follows:

$$n = \frac{\sigma_{0,Ed}}{f_{y0}} \quad (6)$$

For $n < 0$ (compression):

$$k_n = 1.3 - \frac{0.4 \cdot n}{\beta} \leq 1.0 \quad (7)$$

For $n \geq 0$ (tension):

$$k_n = 1.0 \quad (8)$$

In addition, the local buckling resistance of the brace must be checked with the aid of Equations (9), (10) and (11):

$$N_{LB} \geq N_{1,Ed} \quad (9)$$

$$N_{LB} = f_{y1} \cdot t_1 \cdot [2 \cdot h_1 - 4 \cdot t_1 + 2 \cdot b_e] \quad (10)$$

$$b_e = \frac{10}{t_0} \cdot \frac{f_{y0} \cdot t_0}{f_{y1} \cdot t_1} \cdot b_1 \quad (11)$$

where f_{y1} is the brace yield stress

However, these equations were calibrated for carbon steel joints and don't consider the stainless-steel material nonlinearity and strain hardening capacity. Feng and Young [9] proposed equations that better describe the behaviour of cold-formed stainless-steel tubular T-joints. In this case, the chord side wall failure or a combined failure of the chord connected face and the chord side wall can control the design. Equations (12) to (15) were proposed for stainless-steel joints:

$$N_{1np} \geq N_{1,Ed} \quad (12)$$

$$N_{1np} = \min(N_B, N_{LB}) \quad (13)$$

$$N_B = \alpha_B \cdot N_{1,Rd} \quad (14)$$

$$\alpha_B = \frac{2}{25} \left(\frac{h_0}{t_0} - 1 \right) \quad (15)$$

According to the actual design rules present in Eurocode 3 [4], the brace effective width b_e (Equation 11) can't be higher than b_1 , but according to Feng and Young [9], if $\tau = t_1/t_0 \leq 0.55$ it can be considered if the brace local buckling strength (Equation 10) is higher than the brace internal axial force design value.

3 Finite element modelling

3.1 General

Four different tubular T-joints were modelled with the finite element software ABAQUS [12], each with a different 2γ value ranging from 13.3 to 40, with various levels of chord preloads. Only SHS sections were used for the chords and braces. The load-displacement nonlinear analysis was performed using the (*STATIC) procedure in the ABAQUS software. Both the geometric and physical material nonlinearities were considered to model stainless steel behaviour. Aiming a low computational time with accurate results, shell elements were adopted for the brace and chord modelling and the size of the elements varied with the size of the joint. The finite element analysis included some essential factors, such as the modelling of the nonlinear material behaviour and welds, the interaction between the members and the welds and the boundary conditions following the experiments tested by Feng and Young [8]. The dimensions of the finite element models are detailed in

Table 2 where for each joint, different values of chord preload will be considered. According to Feng and Young [8], to ensure that the stresses at the brace and chord intersection are not affected by the ends of the chord, the length of the chord member (L_0) was chosen as $5 \cdot h_0 + h_1$. Still following Feng and Young [8] recommendations, the length of the brace member (L_1) was chosen as $2.5 \cdot h_1$ to avoid the overall buckling of brace members, which cannot reveal the true ultimate capacity of the tubular joints.

To better identify each numerical model, they were labelled according to their cross-section dimensions and their level of chord applied load corresponding to a percentage of chord yield resistance. For example, the label "C80 x 2-B80 x 2-50c" defines the following welded tubular T-joint:

- The letter C refers to chord member followed by the expression "80 x 2" that indicates the dimensions of the cross-section, i.e., chord width and height of 80 mm and a wall thickness of 2 mm;
- The letter B refers to brace member following the same definitions of the chord member;
- The number 50 refers to the percentage of chord applied load correspondent to its yield resistance;
- Finally, the letters "c" (and "t") after 50 means that a compression (or tension) force acts on the chord.

3.2 Finite element type and mesh size

A four-node doubly curved shell element was used with reduced integration (S4R), and a nine-point Simpson integration was applied through the shell thickness. Although the shell element can incorrectly allow the penetration of one member into the other due

to its unawareness of the physical thickness, it still provides an accurate solution to most applications with a low cost in terms of computational time.

A convergence study was carried out to obtain the optimum finite element mesh size. For the smaller specimens, a mesh with approximately 10 mm x 10 mm (width by height) fitted well in modelling the flat portions of either brace and chord. For the larger specimens, a mesh with 8 mm x 8 mm elements was used. At the corner portions, a finer mesh was adopted with four elements for the larger specimens and with three elements for the smaller. Figure 2 depicts the adopted welded tubular T-joints finite element mesh.

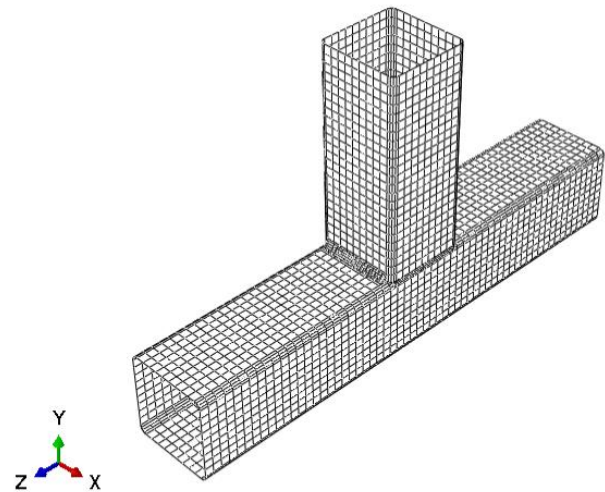


Figure 2 Finite element mesh of welded tubular T-joint C80 x 2-B80 x 2-0

3.3 Material modelling

The austenitic stainless steel mechanical properties obtained by Feng and Young [8] based on stress-strain curves of the tensile coupon tests are shown in

Table 3 and they were used in the finite element models of this study. The static stress-strain curves were determined using the static loads near the proportional limit stress and the ultimate tensile stress. The first portion of the curve represents the material elastic behaviour being determined by Young's modulus (E), and the Poisson's ratio equals to 0,30. The geometric nonlinearity was considered by activating the nonlinear analysis in ABAQUS while the material nonlinearity was introduced with the true stress x true strain curve. The true stress (σ_{true}) and the logarithmic plastic strain (ϵ_{ln}^{pl}) were calculated based on the recommendation of ABAQUS Analysis user's manual [12] as follows:

$$\sigma_{true} = \sigma \cdot (1 + \epsilon) \quad (16)$$

$$\epsilon_{ln}^{pl} = \ln(1 + \epsilon) - \frac{\sigma_{true}}{E} \quad (17)$$

where σ and ϵ in Equations (16) and (17) are the measured stress and strain, respectively. With the stress-strain curve data provided by Feng and Young [8], the engineering curves were approximated based on the Ramberg Osgood method - Equations (18) to (23), as indicated in the Design Manual for Structural Stainless Steel [13].

Table 2 Adopted numerical models dimensions

Numerical models	2γ	Chord (mm)					Brace (mm)					Weld (mm)
		L ₀	h ₀	b ₀	t ₀	r ₀	L ₀	h ₀	b ₀	t ₀	r ₀	w
C40 x 3-B40 x 3-0	13.33	238	40	40	3	2	98	40	40	3	2	5.6
C40 x 2-B40 x 2-0	20.00	238	40	40	2	2	98	40	40	2	2	5.6
C80 x 3-B80 x 3-0	26.66	483	80	80	3	4	193	80	80	3	4	5.8
C80 x 2-B80 x 2-0	40.00	483	80	80	2	4	193	80	80	2	4	5.8

Table 3 Mechanical properties of stainless steel tubes

Section (h × b × t)	E (GPa)	σ _p (MPa)	σ _{0.1} (MPa)	σ _{0.2} (MPa)	σ _{0.5} (MPa)	σ _{1.0} (MPa)	σ _u (MPa)	ε _f (%)
40 x 40 x 2*	194	140	411	447	476	491	704	61
40 x 40 x 3	194	140	411	447	476	491	704	61
80 x 80 x 2*	201	120	360	398	426	438	608	59
80 x 80 x 3	201	120	360	398	426	438	608	59

*Obtained from Feng and Young [8].

The Ramberg Osgood method is presented below:

For $\sigma < f_y$:

$$\varepsilon_{el} = \frac{\sigma}{E} + 0.002 \cdot \left(\frac{\sigma}{f_y}\right)^n \quad (18)$$

For $\sigma > f_y$:

$$\varepsilon_{pl} = 0.002 + \frac{f_y}{E} + \frac{\sigma - f_y}{E_y} + \varepsilon_u \cdot \left(\frac{\sigma - f_y}{f_u - f_y}\right)^m \quad (19)$$

where ε_{el} and ε_{pl} are the elastic and plastic strain, respectively, and ε_u (ultimate strain), n (Ramberg Osgood parameter), m and E_y can be determined by:

$$\varepsilon_u = \frac{f_y}{f_u} \quad (20)$$

$$n = \frac{\ln(4)}{\ln\left(\frac{f_y}{Rp_{0.05}}\right)} \quad (21)$$

$$m = 1 + 2.8 \cdot \left(\frac{f_y}{f_u}\right) \quad (22)$$

$$E_y = \frac{E}{1 + 0.002 \cdot n \cdot \left(\frac{E}{f_y}\right)} \quad (23)$$

where $Rp_{0.05}$ is the 0.05% proof stress.

3.4 Modelling of the welds

The AWS A5.11 [14] specification was adopted to determine the E308L-17 weld properties which were used by Feng and Young [8] in their experimental investigation of cold-formed stainless-steel tubular T-joints. The weld itself consists of three-dimensional solid

elements, with 8-node and reduced integration (C3D8R). The weld geometry was modelled following Figure 3. The considered element mesh size for the weld was 2 mm x 2 mm since the weld stiffness is more significant than that of the members so it was modelled with a finer mesh and was adopted as the master in its contact with the brace and the chord. Extra care was also taken into account to make the meshes on both sides of the weld symmetrical, to avoid irregularities in the loading transmission.

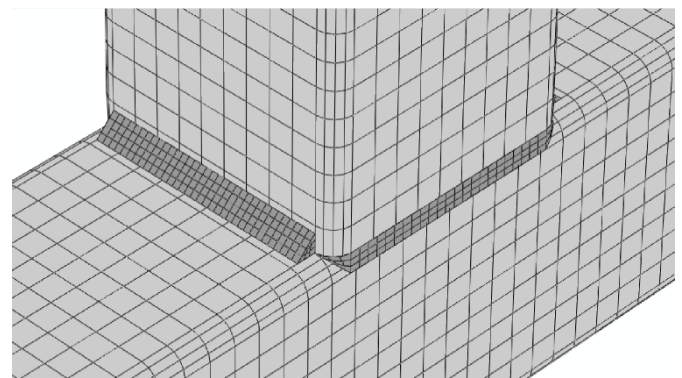


Figure 3 Finite element mesh of welds used in the assessed tubular T-joint

3.5 Loading and boundary conditions

For the modelling of welded tubular T-joints, reference points were created and attached at the top of the brace and the chord ends. These regions were modelled as rigid bodies and restrained against all degrees of freedom of the displacement, except for the displacement at the loaded end in the applied load direction. Furthermore, the lower chord face ends were restrained against displacements in the applied load direction along its entire length.

Figure 4 shows the stainless-steel T-joints boundary conditions adopted in the numerical analysis. The contact between the welds and the members was modelled by using a tie constraint available in ABAQUS. This tool ties two separate surfaces together so that there is no relative motion between them. This type of constraint allows the merge of two regions even though the meshes created on the surfaces of the region are different. It was also necessary to correctly define a master and a slave surface to avoid penetration, so the more refined mesh surface was defined as the master. In this case, the weld surfaces were defined as masters, since its material is stiffer and requires a finer mesh. The loads were applied in increments by using the (*STATIC) method available in the ABAQUS library. The nonlinear geometry parameter (*NLGEOM) was used for considering a large displacement analysis. In the first step, the chord member was directly preloaded to the prescribed load level. This preload level was maintained constant while the brace was loaded using an equivalent displacement. All loads were applied to the members respective reference points and transmitted to its end faces. The total time period of each step was equal 1.

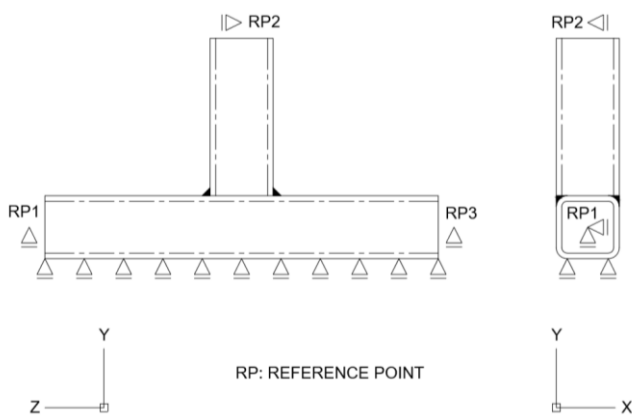


Figure 4 Finite element mesh of the welded tubular T-joint

3.6 Finite element model calibration

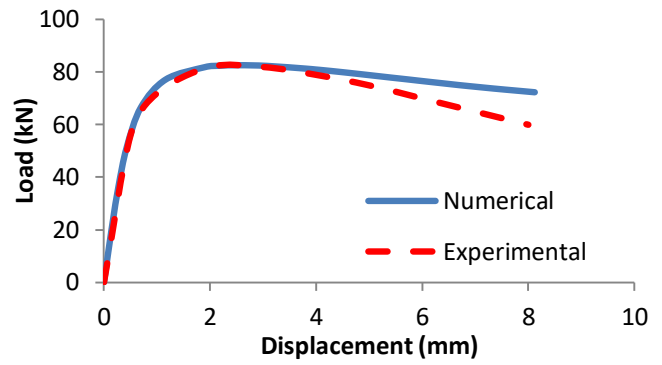
To guarantee the numerical model calibration, a comparison between the experimental results conducted by Feng and Young [8] and the numerical results were carried out to verify the accuracy of the finite elements models, Figure 5.

The non preloaded chord joints with 2 mm thickness wall presented by Feng and Young [8]-[9] were used in this study. These joints were compared in terms of load x displacement curves, where the displacement considered is that which occurs at side wall, since the maximum deformation allowed can't be higher than $3\%b_0$. In both cases, the numerical curves well describe the behaviour of the joints until the chord $3\%b_0$ displacement or the peak loads as obtained in the experimental investigation performed by Feng and Young [8]-[9]. In terms of the deformed shapes, a good agreement was also obtained as can be observed in Figure 6, where the results of the side wall failure modes are presented.

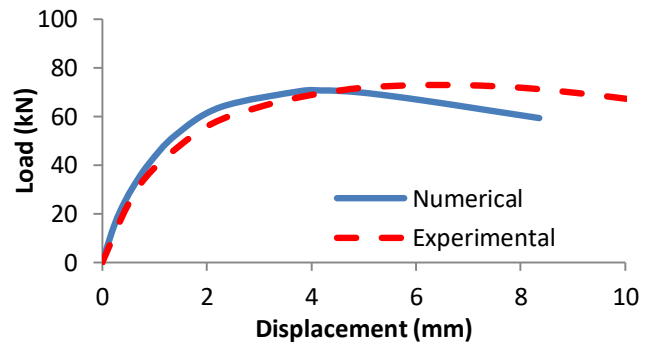
4 Parametric study

4.1 General

The finite element models proved to accurately describe the material behaviour and give a good prediction of the peak load in the cases where the chord is not loaded. Therefore, a parametric study was carried out on aiming the better understand the influence of the chord preload in the stainless steel T-joints overall behaviour. A total of 36 T-joints were analysed in this parametric study, in which 4 of these joints don't have their chords preloaded.



a) T-joint C40x2-B40x2-0

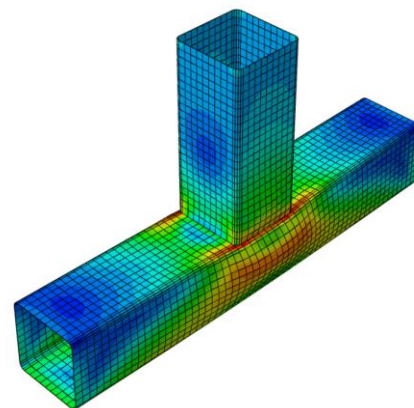


b) T-joint C80x2-B80x2-0

Figure 5 Comparison of experimental and finite element analysis load versus chord side wall displacement curves



a) experimental deformed shape [9]



a) numerical deformed shape

Figure 6 Deformed shapes comparison for chord side wall failure mode for stainless steel T-joints

4.2 Analysed parameters

In the parametric analysis, four different levels of chord preload forces were considered for tension and compression to investigate their influence in the behaviour of the joints. The adopted chord preloads were $0,3 \cdot A\sigma_{0,2\%}$, $0,5 \cdot A\sigma_{0,2\%}$, $0,7 \cdot A\sigma_{0,2\%}$ and $0,9 \cdot A\sigma_{0,2\%}$. The geometric parameter that most influences the joint behaviour against the loaded chord ends was the chord width to chord thickness ratio ($2\gamma = h_0/t_0$). Hence as mentioned before, four different joints were studied with different values for the parameter 2γ , i.e., 13.33, 20.00, 26.66 and 40, respectively. Following the labelling, the rule described at item 3.1, C80 x 2-B80 x 2-0 and C40 x 2-B40 x 2-0 models, that were calibrated with Feng and Young [8], [9] experiments. From these models, the C80 x 2-B80 x 3-0 and the C40 x 2-B40 x 3-0 models were developed with a similar mesh. The validity range of these parameters defined in the Eurocode 3 part 1.8 [4], as well as those in the parametric study is summarised in Table 1. To better understand the joints overall response, the parameter 2γ in the parametric study is purposely designed beyond the validity range defined in the current design specifications, as well as the brace and chord wall thickness, whose lowest value allowed by the current rule is of 2.5 mm.

4.3 Numerical results

The results obtained by the numerical study are presented in Figure 7 and Figure 8 in terms of the load versus side wall displacement

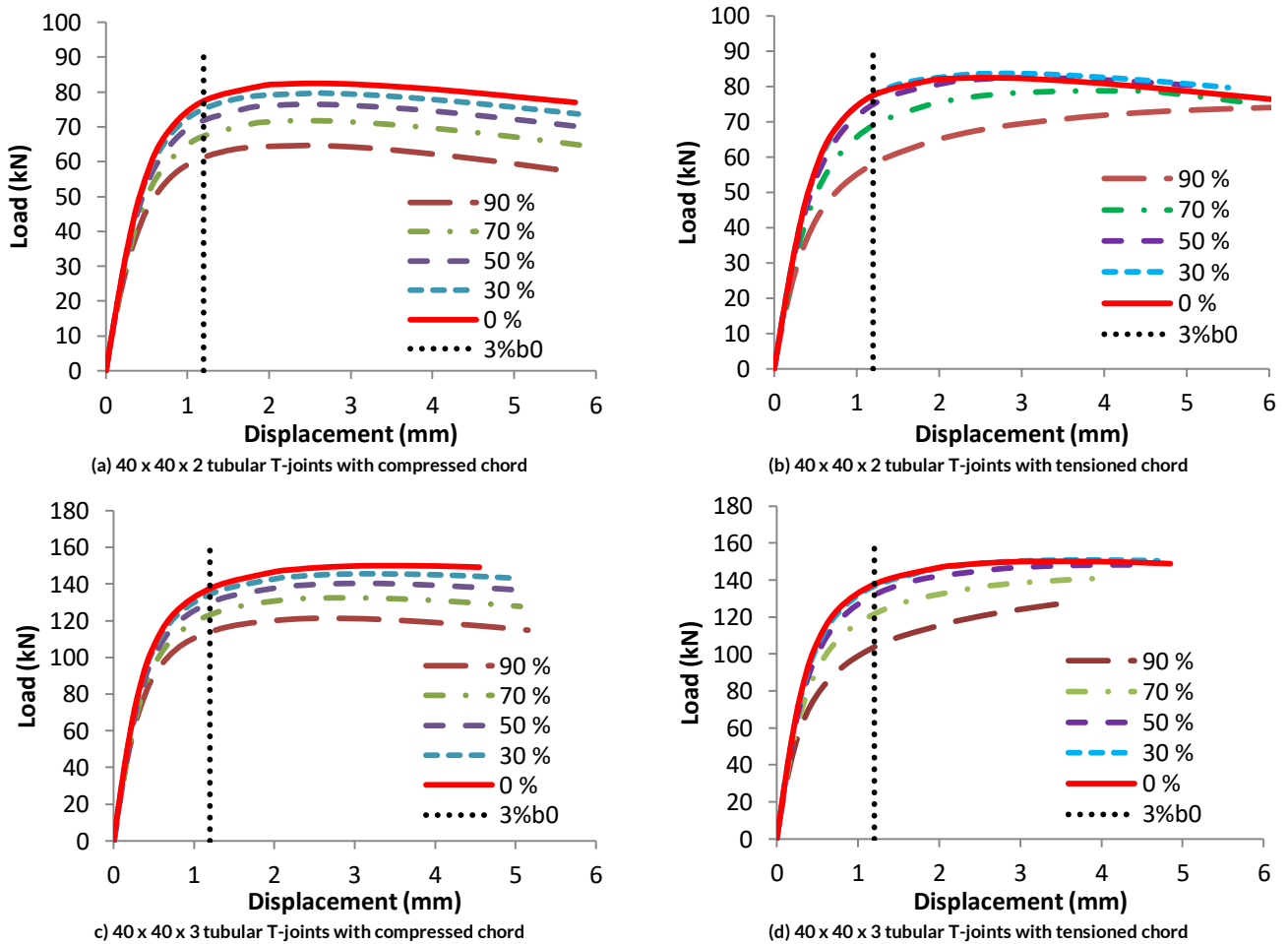


Figure 7 Influence of the chord preload in the stainless steel tubular T-joint overall behaviour – cross-sections 40x40x2 and 40x40x3

curves. These results are summarised in Table 4 and compared to the Eurocode 3 part 1.8 [4], and the Feng and Young's [9] proposed design formulae. The joint numerical strength is obtained from the deformation limit criteria of $3\%b_0$ or peak load [15]. Actually, for the tubular joints that fail by chord side wall failure mode, if the peak load occurs before of a deformation smaller than $3\%b_0$, this peak load is considered as the joint resistance (N_n). On the other hand, if the peak load is reached at a deformation higher than $3\%b_0$, the maximum joint resistance is considered to be the strength at a deformation of $3\%b_0$. For tubular T-joints with brace width to chord width ratio (β) equals 1, as mentioned before, the chord side wall failure mode is expected to occur; as shown in Figure 6. This failure mode was observed in all numerical models assessed in this work.

From the observation of Figure 9 where the joint resistance is presented in terms of the chord stress level parameter n and the ratio between joints with chord preload and joints without chord preload, it may be concluded that there is a slight increase of the joint resistance when it is subjected to chord tension load before it decreases. It is also possible to observe that this effect increases as the parameter 2γ get higher. On the other hand a more significant decrease was observed for the application of compression than for tension forces at the chord, and this effect also increases with the increase of the parameter 2γ .

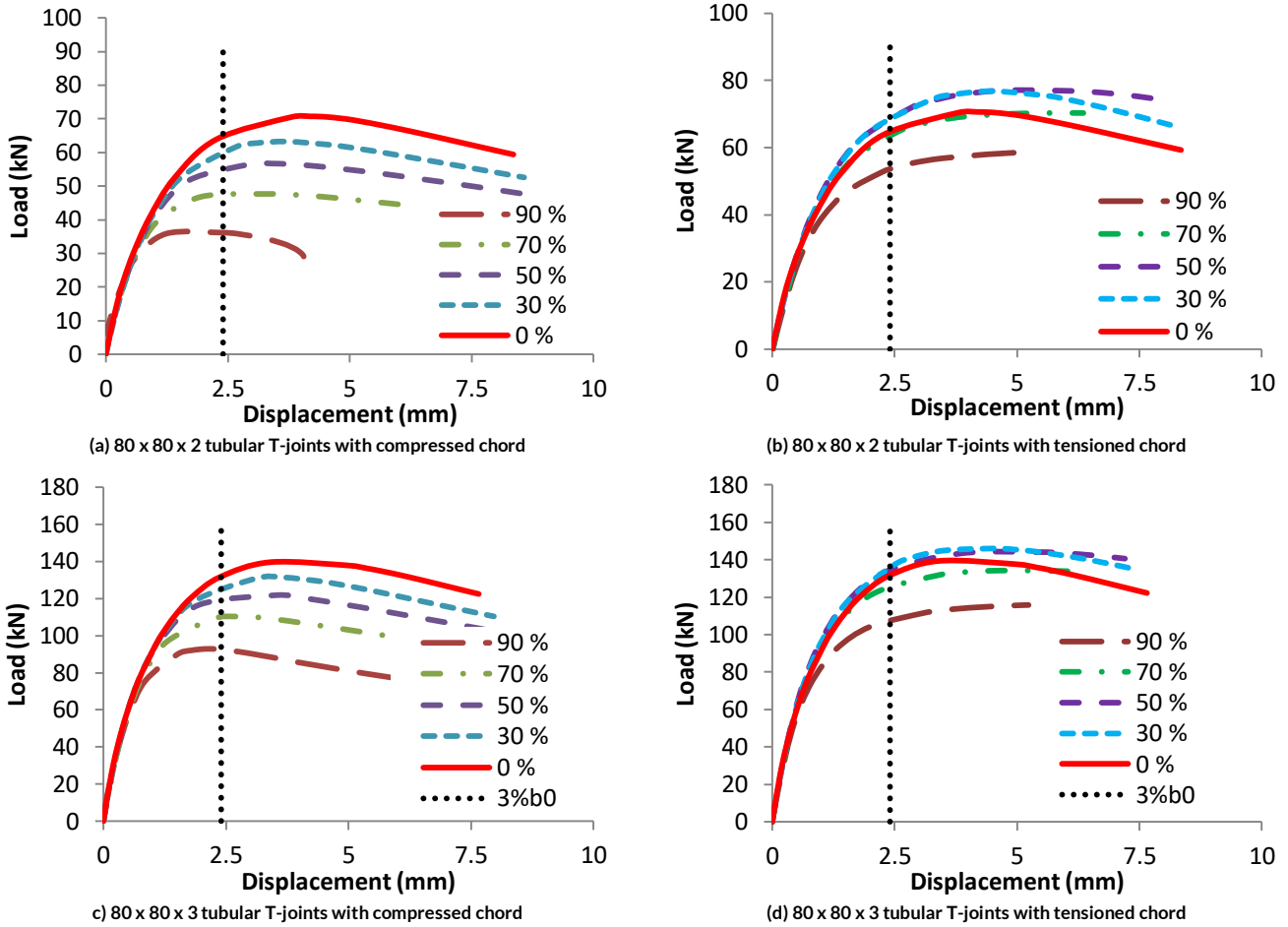


Figure 8 Influence of chord preload in the stainless steel tubular T-joint overall behaviour– cross-sections 80x80x2 and 80x80x3

This result can be explained with the evolution of von Mises stresses on the chord sidewall failure region. In models with chord compression forces, higher stress levels are developed than in the models with tension forces as can be observed in Figure 9.

nonlinearities of stainless steel were included in the models and the numerical results agreed well with the tests performed by Feng and Young [8]. These models were used in the preloaded chord joints analyses. A parametric study was performed using the developed models to better understand the influence of chord loading on the overall behaviour of T-joints. The comparison between the values obtained by the numerical analysis, the current Eurocode 3 rules and the proposed rules reveals that the current equations are not effective for joints with the parameter 2γ much higher than 20. Therefore, the behaviour of the tubular joint with a chord preloaded is not well predicted by the current rules, given that the calculated resistance for tensioned chord joints is the same as those non-loaded chord joints. Additionally, the resistance decrease of compressed chord joints do not follow the actual joint behaviour while varying the 2γ parameter current design rules for carbon steel tubular T-joints with $\beta = 1.0$ are slightly conservative for stainless steel tubular T-joints with low chord width to chord thickness ratio.

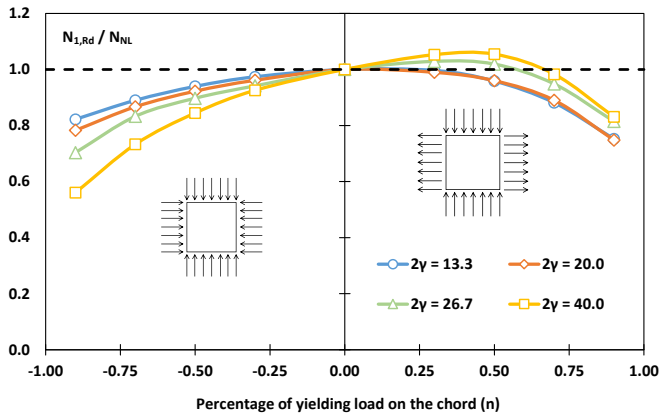


Figure 9 Ratio $N_{1,Rd}/N_{NL}$ versus chord stress level curves of the investigated T-joints, where N_{NL} is the numerical resistance obtained for no loaded chord joints

5 Conclusions

Stainless steel cold-formed SHS tubular T-joints with $\beta = 1.0$ have been investigated by a numerical study. The geometric and material

A further experimental investigation will be performed in the laboratory to better understand the austenitic stainless steel tubular T-joints subjected to chord axial forces. For carbon steel, some experimental evidence from previous research conducted by the authors of the present paper has shown that the design rules for T-joints with chord axial effects are not adequate and need to be modified [16],[17].

Table 4 Comparison of numerical results with code design strengths

Model	2γ	Numerical Strength N_n (kN)	Eurocode 3 $N_{1,Rd}$ (kN)	Proposed strength $N_{1,np}$ (kN)	Comparison	
					$N_n/N_{1,Rd}$	$N_n/N_{1,np}$
C40 x 3-B40 x 3-0	13.3	137.2	107.3	105.9	1.28	1.30
C40 x 3-B40 x 3-30c	13.3	133.6	84.3	83.2	1.58	1.61
C40 x 3-B40 x 3-50c	13.3	128.9	84.3	83.2	1.53	1.55
C40 x 3-B40 x 3-70c	13.3	122.1	84.3	83.2	1.45	1.47
C40 x 3-B40 x 3-90c	13.3	112.8	79.3	78.2	1.42	1.44
C40 x 3-B40 x 3-30t	13.3	136.7	107.3	105.9	1.27	1.29
C40 x 3-B40 x 3-50t	13.3	131.5	107.3	105.9	1.23	1.24
C40 x 3-B40 x 3-70t	13.3	120.9	107.3	105.9	1.13	1.14
C40 x 3-B40 x 3-90t	13.3	103.2	107.3	105.9	0.96	0.97
C40 x 2-B40 x 2-0	20.0	77.3	71.5	108.7	1.08	0.71
C40 x 2-B40 x 2-30c	20.0	74.3	40.7	61.8	1.83	1.20
C40 x 2-B40 x 2-50c	20.0	71.3	40.7	61.8	1.75	1.15
C40 x 2-B40 x 2-70c	20.0	67.0	40.7	61.8	1.65	1.08
C40 x 2-B40 x 2-90c	20.0	60.5	38.2	58.1	1.58	1.04
C40 x 2-B40 x 2-30t	20.0	76.5	71.5	108.7	1.07	0.70
C40 x 2-B40 x 2-50t	20.0	74.2	71.5	108.7	1.04	0.68
C40 x 2-B40 x 2-70t	20.0	68.8	71.5	108.7	0.96	0.63
C40 x 2-B40 x 2-90t	20.0	57.8	71.5	108.7	0.81	0.53
C80 x 3-B80 x 3-0	26.7	131.5	191.1	392.3	0.69	0.34
C80 x 3-B80 x 3-30c	26.7	123.8	82.1	168.6	1.51	0.73
C80 x 3-B80 x 3-50c	26.7	118.0	82.1	168.6	1.44	0.70
C80 x 3-B80 x 3-70c	26.7	109.5	82.1	168.6	1.33	0.65
C80 x 3-B80 x 3-90c	26.7	92.5	77.2	158.4	1.20	0.58
C80 x 3-B80 x 3-30t	26.7	135.3	191.1	392.3	0.71	0.34
C80 x 3-B80 x 3-50t	26.7	134.0	191.1	392.3	0.70	0.34
C80 x 3-B80 x 3-70t	26.7	124.7	191.1	392.3	0.65	0.32
C80 x 3-B80 x 3-90t	26.7	107.1	191.1	392.3	0.56	0.27
C80 x 2-B80 x 2-0	40.0	64.4	127.4	397.4	0.51	0.16
C80 x 2-B80 x 2-30c	40.0	59.6	28.2	88.1	2.11	0.68
C80 x 2-B80 x 2-50c	40.0	54.4	28.2	88.1	1.93	0.62
C80 x 2-B80 x 2-70c	40.0	47.2	28.2	88.1	1.67	0.54
C80 x 2-B80 x 2-90c	40.0	36.1	26.5	82.8	1.36	0.44
C80 x 2-B80 x 2-30t	40.0	67.8	127.4	397.4	0.53	0.17
C80 x 2-B80 x 2-50t	40.0	67.9	127.4	397.4	0.53	0.17
C80 x 2-B80 x 2-70t	40.0	63.3	127.4	397.4	0.50	0.16
C80 x 2-B80 x 2-90t	40.0	53.5	127.4	397.4	0.42	0.13

References

- [1] Wardenier, J.; Van Der Vegte, G.J.; Packer, J.A.; Zhao, X.-L. (2010) Background of the New RHS Joint Strength Equations in The New IIW (2009) Recommendations, Proceedings of The 13th. International Symposium on Tubular Structures, Hong Kong, China.
- [2] Gomes N.V.; Lima L.R.O. de; Vellasco P.C.G. da S.; Silva A.T. da; Rodrigues M.C.; Costa-Neves L.F. (2019) Experimental and numerical investigation of SHS truss T-joints reinforced with side-wall plates. *Thin-Walled Structures*, 145: 106404.
- [3] Gardner, L. (2005) The use of stainless steel in structures. *Progress in Structural Engineering and Materials*, 7(2): 45-55.
- [4] EN1993-1-8, Eurocode3-Design of Steel Structures-Structures-Part1-8: Design of Joints, CEN, ECCS, Brussels, 2010.
- [5] ABNT NBR 16239 (2013) Design of steel and composite structures for buildings using hollow sections, Associação Brasileira de Normas Técnicas, São Paulo, Brazil (in Portuguese).
- [6] Packer, J. A., Wardenier, J., Zhao, X.-L., Vegte, G. J. van der, Kurobane, Y. (2009). Design guide for rectangular hollow section (RHS) joints under predominantly static loading. 2nd Edition, Construction with hollow steel sections, No. 3, CIDECT.
- [7] ISO 14346 (2013) Static design procedure for welded hollow-section joints – Recommendations, International Organization for Standardization, Switzerland.
- [8] Feng, R., & Young, B. (2008) Experimental investigation of cold-formed stainless steel tubular T-joints. *Thin-Walled Structures*, 46(10): 1129-1142.
- [9] Feng, R., & Young, B. (2011) Design of cold-formed stainless steel tubular T-and X-joints. *Journal of Constructional Steel Research*, 67(3): 421-436.
- [10] Packer, J. A.; Wardenier J.; Kurobane Y.; Dutta D.; Yeomans N. (1992) Design guide for rectangular hollow section (RHS) joints under predominantly static loading. In: Comité International pour le Développement et l'Étude de la Construction Tubulaire (CIDECT). Velarg TÜG Rheinland, Cologne, Germany.
- [11] EN 1993-1-1. Eurocode 3-Design of steel structures - Part 1-1: general rules and rules for buildings. European Committee for Standardization, EN 1993-1-1, CEN. Brussels, Belgium; 2003.
- [12] ABAQUS Inc S. ABAQUS Analysis user's manual. 614th ed, 2014
- [13] SCI 2017, Design Manual for Structural Stainless Steel, 4th Edition, Ascot, UK: The Steel Construction Institute.
- [14] American Welding Society (AWS). Specification for nickel and nickel-alloy welding electrodes for shielded metal arc welding. AWS A5.11M. Miami (USA); 2005.
- [15] Zhao X.L., Wardenier J., Packer J.A., van der Vegte G. J., Current static design guidance for hollow-section joints, *Structures and Buildings*. 163 (2010) SB6: 361-373.
- [16] Nizer, A; Lima, L. R. O. De; Vellasco, P. C. G. Da S; Andrade, S. A. L. De; Goulart, E. Da S; Silva, A. T; Neves, L. F. Da C. Experimental and Numerical Assessment of T RHS Joints Subjected to Brace and Chord Axial Forces. *Steel Construction & Design and Research*, v. 9, p. 315-322, 2016.
- [17] Lima, L. R. O. de; Vellasco, P. C. G. da S. ; Silva, A. T. ; Rodrigues, M. C. ; Neves, L. F. Da C. ; Guerreiro, L. C. B. ; Mendes, F. F. . Recent advances in tubular joints experiments in Brazil. *Stahlbau*, v. 87, p. 355-362, 2018.